# Dual-laser absorption spectroscopy of $C_2H_2$ at 1.4 $\mu$m

E. Fasci,[1] T. A. Odintsova,[1] A. Castrillo,[1,*] M. D. De Vizia,[1] A. Merlone,[2] F. Bertiglia,[2] L. Moretti,[1] and L. Gianfrani[1,†]
[1]*Dipartimento di Matematica e Fisica, Seconda Università di Napoli, Viale Lincoln, 5 I-81100 Caserta, Italy*
[2]*Istituto Nazionale di Ricerca Metrologica, Strada delle Cacce, 91 I-10135 Torino, Italy*
(Received 4 March 2016; published 28 April 2016)

Spectroscopic parameters (line intensity factor, pressure self-broadening, and shifting coefficients) of $C_2H_2$ at 1.4 $\mu$m were accurately measured using a dual-laser approach, based upon the technique of optical phase locking. This generated an absolute frequency scale underneath the absorption spectra. A pair of extended-cavity diode lasers was used. One of them, the probe laser, is forced to maintain a precise frequency offset from a reference laser, which is an optical frequency standard based on noise-immune cavity-enhanced optical heterodyne molecular spectroscopy. Laser-gas interaction takes place inside an isothermal multipass cell that is stabilized at the temperature of the triple point of water. The fidelity in the observation of the shape associated to the $P_e(14)$ line of the $2\nu_3 + \nu_5$ band allowed us to measure the spectroscopic parameters, with a global uncertainty for the line strength of 0.22%.

DOI: 10.1103/PhysRevA.93.042513

## I. INTRODUCTION

Acetylene ($C_2H_2$), also known as ethyne, is one of the most important nonmethane hydrocarbons (NMHCs). Its spectroscopic parameters are crucial in several research fields, such as combustion science, astrophysics, and Earth and planetary atmospheric chemistry. Acetylene is a minor constituent of our atmosphere [1,2] as well as of the atmospheres of Mars [3], Jupiter [4], Titan [5], Uranus [6,7], and Neptune [8]. It significantly contributes to the opacities of stars and plays a central role in the synthesis of various important astronomical relevant species [9]. Furthermore, its crucial presence in some star-forming regions of the interstellar space has been shown [10].

Acetylene is one of the longest-lived NMHCs, with a mixing ratio in the range of 500–3000 ppt and an average tropospheric lifetime of the order of two months, allowing this compound to reach remote areas as well as the stratosphere. Its destruction in the Earth's atmosphere occurs by reaction with OH radicals, ozone, and other oxidants. In light of that, its influence on the Earth's climate is quite significant and accurate reconstructions of vertical profiles of this trace gas are of particular relevance. In fact, acetylene has been used as a reliable tracer for anthropogenic emissions since it is mostly derived from human activities related to combustion of hydrocarbon, fossil and bio fuels and from biomass burning. $C_2H_2$ is often used as an indicator of combustion sources and as a tracer for atmospheric transport processes and chemistry (see [11] and references therein). Furthermore, it has been shown that acetylene is also produced to a lesser extent by natural processes in oceanic water, and, even though this process at the present age is not predominant, it must be accounted for to explain the presence of $C_2H_2$ in air bubbles stored in ancient ices [12].

As a matter of fact, quantitative information on $C_2H_2$ densities in a variety of environments is extremely important. Their retrieval from $C_2H_2$ spectra requires the precise knowledge of line positions, integrated intensities, broadening and shifting coefficients.

Acetylene has also attracted the interest of the International Committee for Weights and Measures because of its relatively strong absorption features in the International Telecommunication Union's C band (1530–1560 nm). In fact, a large variety of rovibrational $C_2H_2$ lines have been used as secondary frequency standards for the important field of optical telecommunications [13,14] and the strongest lines of the near-infrared spectrum have been extensively measured by using the modern technology of optical frequency comb synthesizers [15–17]. In addition, $C_2H_2$ is being used as a molecular target for the spectroscopic determination of the Boltzmann constant by means of Doppler Broadening Thermometry (DBT) (see [18] and reference therein).

In the last few years, spectroscopic data regarding the near-infrared spectrum of acetylene have been noticeably enriched, especially in six different spectral regions, namely, around 3, 2.2, 1.9, 1.7, 1.5, and 1.4 $\mu$m [19]. Many efforts have been made in this field, using well-consolidated spectroscopic techniques, such as high-resolution Fourier transform spectrometry [20,21], direct laser absorption spectroscopy [22], and cavity ring-down spectroscopy [23]. Interesting results have been also obtained by using spectroscopic techniques assisted by the technology of optical frequency combs [24,25]. In most of these studies, the Voigt profile (VP) has ben adopted for the aims of the spectral analysis. Nevertheless, highly accurate experiments have already demonstrated the VP inadequacy. In fact, the VP takes into account Doppler and collisional broadenings, thus neglecting second-order effects such as the speed dependence of relaxation rates and the averaging effect of velocity-changing collisions. A wide variety of models have been proposed to consider these narrowing effects [26]. Very recently, a task group of the International Union of Pure and Applied Chemistry has suggested the use of a new profile, named the Hartmann-Tran profile (HTP) [27]. This profile, also known as the partially correlated quadratic speed-dependent hard collision profile or the partially correlated quadratic speed-dependent Nelkin—Ghatak profile, is sophisticated enough to include the two narrowing mechanisms and their physical correlations, while

*Corresponding author: antonio.castrillo@unina2.it
†Correspondence can be also sent to livio.gianfrani@unina2.it

 

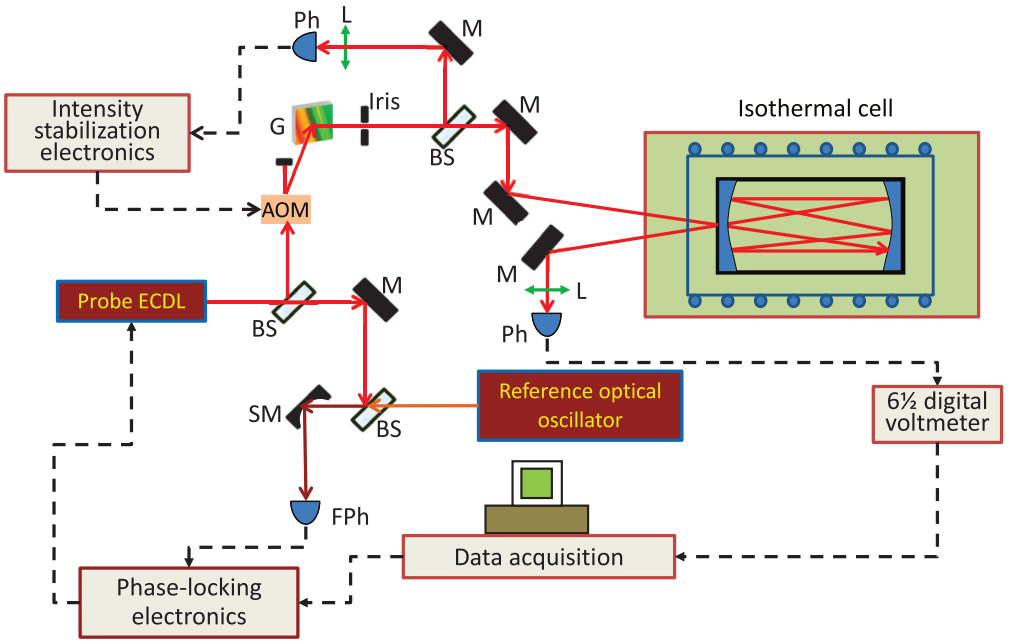


FIG. 1. Sketch of the dual-laser spectrometer. BS, beam splitter; M, mirror; SM, spherical mirror; G, grating; L, anti-reflection coated lens; AOM, acousto-optic modulator; Ph, InGaAs photodiode; FPh, fast photodiode.

being very efficient to be computed [28]. The HTP model has been recently tested on $H_2O$ [29,30], $CO_2$ [31], $O_2$ [32], and CO [33] spectra, giving results that are consistent with more sophisticated models. Concerning acetylene, the HTP model has been successfully applied just in one case, at 1.5 $\mu$m, in coincidence with the $P_e(11)$ line of the $\nu_1 + \nu_3$ band [34].

In this work, using an absorption spectrometer based upon a pair of phase-locked extended-cavity diode lasers, we measured the $P_e(14)$ line of the $2\nu_3 + \nu_5$ band, at pressures ranging between 3 and 30 Torr (i.e., roughly 400–4000 Pa) and at the constant temperature of the triple point of water (273.16 K). The spectrometer allowed us to perform highly accurate and reproducible frequency scans around a given center frequency. This feature, in conjunction with the linearity of the detection chain, made it possible to avoid any instrumental distortion in measuring absorption line shapes, reaching an experimental accuracy limited only by the noise level. By using the HTP model, the line intensity, self-broadening and self-shifting coefficients were retrieved with a relative uncertainty of about 0.22, 0.13, and 0.18%, respectively.

The paper is organized as follows: Sec. II describes the experimental setup, Sec. III deals with the line-shape model, while the results are presented and discussed in Sec. IV. Conclusions and future studies are the subject of Sec. V.

## II. EXPERIMENTAL DETAILS

The dual-laser spectrometer, schematically reported in Fig. 1, essentially consists of an extended-cavity diode laser (namely, the probe laser) with an emission wavelength in the range between 1.38 and 1.41 $\mu$m, a frequency stabilization and control unit (including a reference laser), an intensity stabilization feedback loop, and an isothermal cell.

The probe laser (PL) was phase locked to the reference laser (RL) by using the phase-locking electronics that is shown in Fig. 2. More specifically, portions of the two laser beams are focused on a fast photodetector (with a bandwidth of 12 GHz) to produce a beat-note signal which is sent to a power amplifier (model RF BAY LPA-8-17), scaled in frequency by a factor of 40 (by using a frequency divider, model RF BAY FPS-40-12), split into two parts and then sent to a pair of digital phase and frequency detectors (PSDs).

The former (PSD1 of Fig. 2, model RF BAY PDF-100) has an integrated loop filter limiting its bandwidth to 10 kHz, while the latter (PSD2, model Analog Devices 9901) is much faster. The first PSD ensured a robust and reliable frequency lock in the audio bandwidth (roughly 1 kHz for the loop controlling the extended cavity length and 10 kHz for that acting on the current driver), whereas the latter ensured an effective phase locking between the two lasers. A radio-frequency (rf) synthesizer (model RHODE&SCHWARZ SMBV100) provides the reference rf signal for both the PSDs, as well as the tunable offset frequency between the two lasers. As a result of the action of the third loop that controls the laser current through a bias tee, a significant narrowing of the

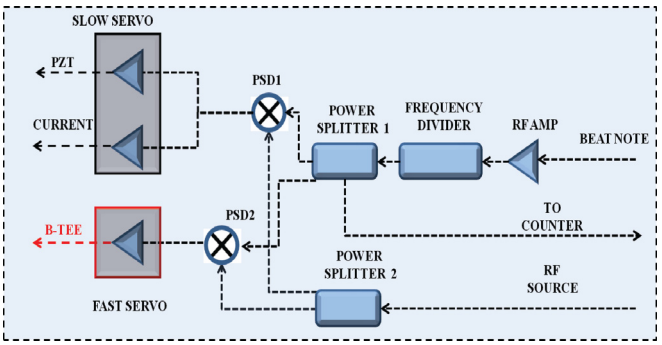


FIG. 2. Block diagram of the phase-locking electronics.

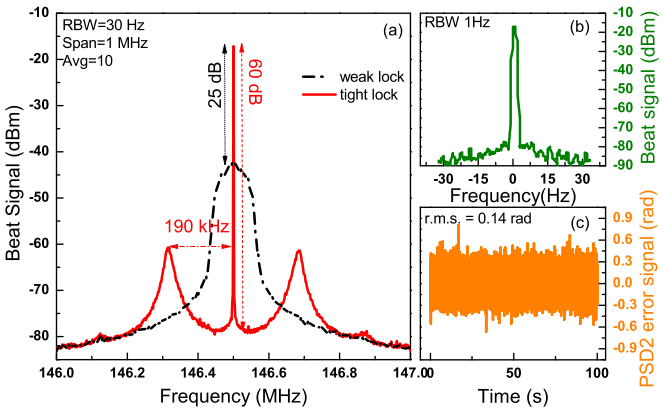


FIG. 3. (a) Example of a beat note between probe and reference lasers under weak (PSD2 deactived) and tight lock (PSD2 actived) conditions. (b) Beat note under tight lock with higher resolution, characterized by a signal-to-noise ratio of 60 dB, which represents an improvement of 25 dB with respect to the weak lock. (c) Error signal recorded at the output of the phase detector AD9901, acquired for a total time of 100 s and with an integration time of 2 ms.

beat-note could be observed, down to the Hz level, as shown in Fig. 3. This demonstrates that the PL spectral purity could be improved up to the limit determined by the RL. In fact, from the error signal generated by PSD2, recorded by means of a digital oscilloscope over a period of 100 s and shown in the third panel (c) of Fig. 3, it was possible to estimate the residual phase fluctuations, the root-mean-square (rms) value of which amounts to 0.14 rad, on a loop bandwidth of about 190 kHz. This was estimated from the servo bumps that appear in the spectral shape of the closed-loop beat-note signal.

The reference laser was an optical frequency standard based on noise-immune cavity-enhanced optical heterodyne molecular spectroscopy (NICE-OHMS) [35]. More specifically, the emission frequency of an extended-cavity diode laser (ECDL) was actively stabilized against the center of a sub-Doppler $H_2{}^{18}O$ line, observed under optical saturation conditions in a high-finesse resonator [36]. We exploited the fact that NICE-OHMS provides a dispersion signal without dithering the optical cavity, likely to be employed as an error signal. The emission line width of the RL was carefully determined from measurements of the frequency-noise power spectral density. It turned out that the linewidth of the optical frequency standard amounts to about 7 kHz (full width at half maximum) for an observation time of 1 ms [37].

Laser-gas interaction takes place inside an isothermal cell, actively stabilized at the temperature of the triple point of water. It consists of a spherical, Herriott-type, multiple reflection cell with a maximum path length of 12 m in a volume of about 400 $cm^3$. The cell is entirely in stainless steel, with electropolished inner and outer cavity surfaces. Temperature control and measurements were done by using a pair of capsule-type standard platinum resistance thermometers (SPRTs, Hart Scientific, model 5686). The two SPRTs are placed inside the cylindrical spacer, into two holes expressly drilled in the front and in the back of the cell, with a displacement of 180°. The resulting displacement of the SPRTs sensing elements allowed for the evaluation of the maximum temperature gradient, since they are positioned in both radial and axially opposite positions. SPRTs were calibrated at the Italian Institute for Research in Metrology in the temperature interval between the triple point of mercury and the indium freezing point. Temperature stability (as determined over one full day at the temperature of the triple point of water) was found to be at the level of 0.1 mK, while temperature homogeneity was better than 1 mK. These extraordinary performances were ensured by a sophisticated system, already described elsewhere [38], essentially made of two cylindrical chambers, one inside the other, the multipass cell being housed inside the inner one. In order to obtain acoustic and thermal insulation from the outside environment, the two chambers were kept under vacuum conditions. Two independent temperature stabilization stages were used: an auxiliary thermostat and a fine heating control, the former acting on the inner chamber (exploiting the circulation of a thermal fluid), the latter on the multipass cell (through a constantan heater wire, uniformly wrapped around the cell body).

As for the intensity stabilization of the probe laser, we adopted the same configuration of past experiments [39–41]. Two identical ultralow-noise 10-kHz bandwidth preamplified InGaAs photodiodes (New Focus, model 2011-FS-M) were used, the former to produce the reference signal that is required for the intensity stabilization, the latter to monitor the power on the output of the isothermal cell. A digital voltmeter, with six and half-digit resolution (Agilent, model 34401A), connected to a personal computer through a USB-GPIB board, was used to measure the transmitted signals.

Highly linear, accurate, and reproducible frequency scans of the PL around a given center frequency were implemented by continuously tuning the rf offset frequency. Details regarding the linearity of the frequency scale, as well as the whole detection chain, will be provided in Sec. IV C. A Labview code was developed to perform the step-by-step frequency scan and to acquire, for each step, the transmitted signal.

The gas pressure was measured by means of a 100-Torr capacitance manometer (model VCMT12TDA from Varian), with an accuracy of 0.25% of the reading. A turbomolecular pump was used to periodically evacuate the isothermal cell and create high-purity conditions. The acetylene sample was in a commercial bottle with a quoted concentration of 99.6%. Unfortunately, the manufacturer did not provide the uncertainty for the gas purity. In the data analysis, it was conservatively set to 1%. Regarding the isotopic content, we assumed that the $C_2H_2$ sample was at the natural abundance, namely, with 97.7599% of $^{12}C_2H_2$.

## III. LINE-SHAPE MODEL

In the last three decades, the line-shape theory has been widely developed and several alternatives to the VP, with increasing complexity, have been proposed [26]. A detailed review is out of the scope of this paper. Here, we just report the main equations that should be considered to generate the HTP profile. Before moving to the equations, it is important to point out that this profile, while accounting for the Dicke narrowing effect, the speed dependence of line broadening and shifting, and the partial correlation between velocity- and phase-changing collisions, offers an important advantage with

respect to other sophisticated models. It can be easily and rapidly computed for two main reasons: (i) it is expressed in terms of only two complex probability functions and (ii) the speed dependence of the relaxation rates is introduced in the framework of the so-called quadratic approximation [42,43].

Introducing eight parameters, namely, the line center frequency $\nu_0$, the Doppler width $\Gamma_D$, the mean collisional relaxation rate $\Gamma_0$, the mean collisional shift of the line center $\Delta_0$, the parameters $\gamma_2$ and $\delta_2$ accounting for the speed dependence of collisional broadening and shifting, the frequency of velocity-changing collisions $\nu_{VC}$, and the $\eta$ parameter representing the partial correlation between velocity and rotational state changes due to collisions, the HTP can be expressed as follows [28]:

$$\mathrm{HTP}(\nu) = \frac{1}{\pi}\mathrm{Re}\left\{\frac{A(\nu)}{1-\left[\nu_{VC}-\eta\left(C_0-\frac{3C_2}{2}\right)\right]A(\nu)+\left(\frac{\eta C_2}{v_{a0}^2}\right)B(\nu)}\right\}. \tag{1}$$

The terms $A(\nu)$ and $B(\nu)$ are combinations of the complex probability function $w(z)$,

$$w(z) = \frac{i}{\pi}\int_{-\infty}^{+\infty}\frac{e^{-t^2}}{z-t}dt = e^{-z^2}erfc(-iz), \tag{2}$$

where *erfc* is the complementary error function, while

$$\begin{aligned} A(\nu) &= \frac{\sqrt{\pi}c}{\nu_0 v_{a0}}\left[w(iZ_-) - w(iZ_+)\right], \\ B(\nu) &= \frac{v_{a0}^2}{\widetilde{C}_2}\left[-1+\frac{\sqrt{\pi}}{2\sqrt{Y}}(1-Z_-^2)w(iZ_-)\right. \\ &\quad \left.-\frac{\sqrt{\pi}}{2\sqrt{Y}}(1-Z_+^2)w(iZ_+)\right]. \end{aligned} \tag{3}$$

In these expressions, the quantities $X$, $Y$, $Z_+$, and $Z_-$ are given by

$$\begin{aligned} Z_\pm &= \sqrt{X+Y}\pm\sqrt{Y}, \\ X &= \frac{i(\nu_0-\nu)+\widetilde{C}_0}{\widetilde{C}_2}, \\ Y &= \left(\frac{\nu_0 v_{a0}}{2c\widetilde{C}_2}\right)^2, \end{aligned} \tag{4}$$

where $c$ is the vacuum speed of light and

$$\begin{aligned} \widetilde{C}_0 &= (1-\eta)\left(C_0-\frac{3C_2}{2}\right)+\nu_{VC}, \\ \widetilde{C}_2 &= (1-\eta)C_2, \\ v_{a0} &= \sqrt{\frac{2k_BT}{M}}. \end{aligned} \tag{5}$$

In this latter equation, $v_{a0}$ represents the most probable speed of the molecules of mass $M$ at temperature $T$, while $k_B$ is the Boltzmann constant. It must be noted that the coefficients $C_0$ and $C_2$ appearing in Eq. (5) can be expressed in terms of $\Gamma_0$, $\Delta_0$, $\gamma_2$, and $\delta_2$, as follows:

$$\begin{aligned} C_0 &= \Gamma_0 + i\Delta_0, \\ C_2 &= \gamma_2\Gamma_0 + i(\delta_2\Delta_0), \end{aligned} \tag{6}$$

where, as suggested by Rohart *et al.* in [42,43], the dependence of the relaxation rates on the molecular speed, $v_a$, is assumed to be

$$\begin{aligned} \Gamma(v_a) &= \Gamma_0\left\{1+\gamma_2\left[\left(\frac{v_a}{v_{a0}}\right)^2-\frac{3}{2}\right]\right\}, \\ \Delta(v_a) &= \Delta_0\left\{1+\delta_2\left[\left(\frac{v_a}{v_{a0}}\right)^2-\frac{3}{2}\right]\right\}. \end{aligned} \tag{7}$$

For the spectral analysis, we implemented a global-fitting procedure [44] inspired by the pioneering work of Benner *et al.* [45]. The global analysis of experimental profiles recorded at different gas pressures is a powerful tool for testing the validity of a line-shape model. Moreover, compared to the usual adjustment of individual spectra, the global procedure has the advantage of strongly reducing the statistical correlation between free parameters. In particular, implementing some physical constraints, it is possible to share a number of free parameters, as will be better explained in the subsequent section. Furthermore, taking advantage of the fact that the gas temperature is known with an extremely high accuracy, the Doppler width $\Gamma_D = \frac{\nu_0}{c}\sqrt{2\ln 2\frac{k_BT}{M}}$ could be fixed at the value corresponding to the measured temperature [0.016665 $\mathrm{cm}^{-1}$, for the $P_e(14)$ line], over the entire pressure range. As for the parameter $\eta$, it was fixed at 0.15, according to the recent findings of [34].

Finally, for the calculation of the complex probability function $w(z)$, we used the MATLAB routine available in [46], which is an improvement of the Weideman approximation [47].

## IV. RESULTS AND DISCUSSION

### A. Data analysis and retrieval of spectroscopic parameters

In Table I, we report some useful information regarding the $C_2H_2$ vibration-rotation transition investigated in the present work. We also report the water line against which the RL was stabilized, along with its frequency distance from the acetylene line.

Figure 4 shows a series of transmission spectra for the $P_e(14)$ line of the $2\nu_3+\nu_5$ $C_2H_2$ band, recorded at the constant temperature of the triple point of water as a function of the gas pressure, which was varied between 3 and 30 Torr. We draw the reader's attention to the occurrence of a weaker absorption line at the low-frequency side of the scan, which is not reported in the HITRAN database [48]. Looking into the line list of [21], it seems clear that such an interfering line is due to the $^{13}CH^{12}CH$ molecule.

On the horizontal axis of Fig. 4, we report the frequency offset of the probe laser with respect to the reference one. In this case, laser scans were 5160 MHz wide and resulted from 1032 steps of 5 MHz each. All the spectra were fitted to the following function:

$$\begin{aligned} P(\nu) &= (P_0+P_1\nu) \\ &\quad\times\exp\left[-A^P g^P\left(\nu-\nu_0^P\right)-A^I g^I\left(\nu-\nu_0^I\right)\right], \end{aligned} \tag{8}$$

where the parameters $P_0$ and $P_1$ account for a possible residual variation of the incident power, $\nu$ represents the frequency detuning from RL, and $A^P$ and $g^P(\nu-\nu_0^P)$ are

TABLE I. Investigated $C_2H_2$ line, with its transition wave number and intensity factor at $T_0 = 296$ K. The reference $H_2$ $^{18}O$ line, belonging to the $\nu_1 + \nu_3$ band, is also reported, along with the frequency separation from the adjacent $C_2H_2$ line. Data are taken from the HITRAN database [48].

| $C_2H_2$ line | Rovibrational band | Number of spectra | Investigated pressures | Frequency ($cm^{-1}$) | Line strength ($10^{-23}$cm/molecule) | Reference $H_2$ $^{18}O$ line | Frequency separation (GHz) |
|---|---|---|---|---|---|---|---|
| $P_e(14)$ | $2\nu_3 + \nu_5$ | 220 | 11 | 7183.390000 | 1.551 | $5_{5,0} \rightarrow 5_{5,1}$ | 5.87 |

the integrated absorbance and the line-shape function of the probed line, respectively. Similarly, the quantities denoted by the superscript $I$ refer to the $^{13}CH^{12}CH$ interfering line. As for the line-shape functions, the HTP model was adopted. In the global fitting procedure, we retained $P_0$ and $P_1$ and the integrated absorbance $A^P$ as free parameters of individual spectra, while $\nu_0^I$ and $\nu_0^P$, $\gamma_0^I$ and $\gamma_0^P$, and $\delta_0^I$ and $\delta_0^P$ were shared across spectra in the whole pressure range, the quantities $\gamma_0$ and $\delta_0$ being the self-broadening and shifting coefficients, respectively. The integrated absorbance of the interfering line, $A^I$, was constrained to be proportional to $A^P$, the proportionality factor being a free parameter, also shared among the various spectra. The two Doppler widths, $\Gamma_D^I$ and $\Gamma_D^P$, were fixed at the expected values. The remaining parameters, $\beta_{VC}$, $\gamma_2$, and $\delta_2$, were set equal for the two lines and shared among the spectra. It should be noted that $\beta_{VC}$ represents the velocity-changing collision frequency per unit of pressure.

Figure 5 shows the residuals resulting from the application of the global-fitting procedure to the seven spectra of Fig. 4. We must note the excellent agreement between the experimental data and the theoretical model, the rms of the residuals ranging from 650 to 900 $\mu$V, mostly limited by the experimental noise. In our experimental conditions, for a laser power of 50 $\mu$W impinging on the detector, we could calculate a voltage shot-noise limit of about 25 nV/$\sqrt{\text{Hz}}$. This value is almost a factor 30 000 lower than the noise observed in the absorption spectra. A possible source of noise could be ascribed to residual laser power fluctuations not properly compensated by the intensity stabilization loop. Extra noise could be also introduced either from unwanted electrical pick-up or from residual mechanical vibrations converted in spurious laser power fluctuations. Moreover, no clear structures could be evidenced. Also, there was no dependence on the gas pressure, a circumstance that demonstrates the capability of the HTP model of modeling the absorption spectra in the entire pressure range. Another argument supporting this conclusion is related to the velocity-changing collision frequency. Several experiments have shown that there exists an upper limitation to this frequency, which is given by the diffusion theory, namely, $\nu_{VC}^{kin} = \frac{k_B T}{MD}$, where $D$ is the mass diffusion coefficient. Furthermore, $\nu_{VC}^{kin}$ is expected to be proportional to the gas pressure, $p$. For acetylene molecules, the diffusion theory predicts that this proportionality factor, at 273.16 K, is equal to 0.03975 $cm^{-1}$/atm [49]. As a matter of fact, for $\eta$ equal to

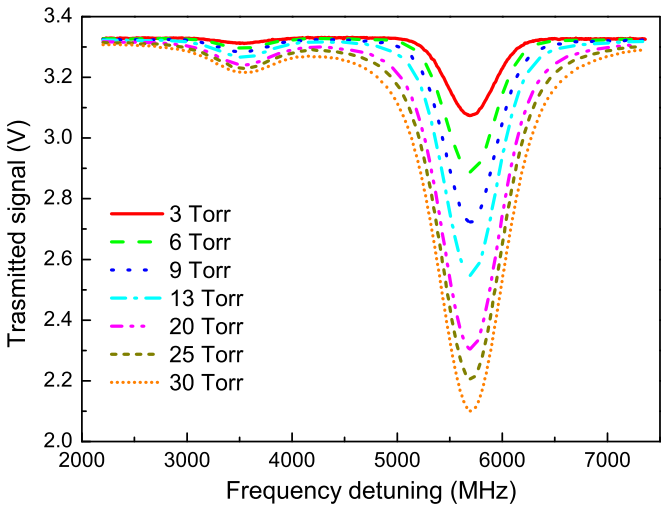


FIG. 4. Examples of absorption spectra relative to the $P_e(14)$ transition acquired as a function of the gas pressure.

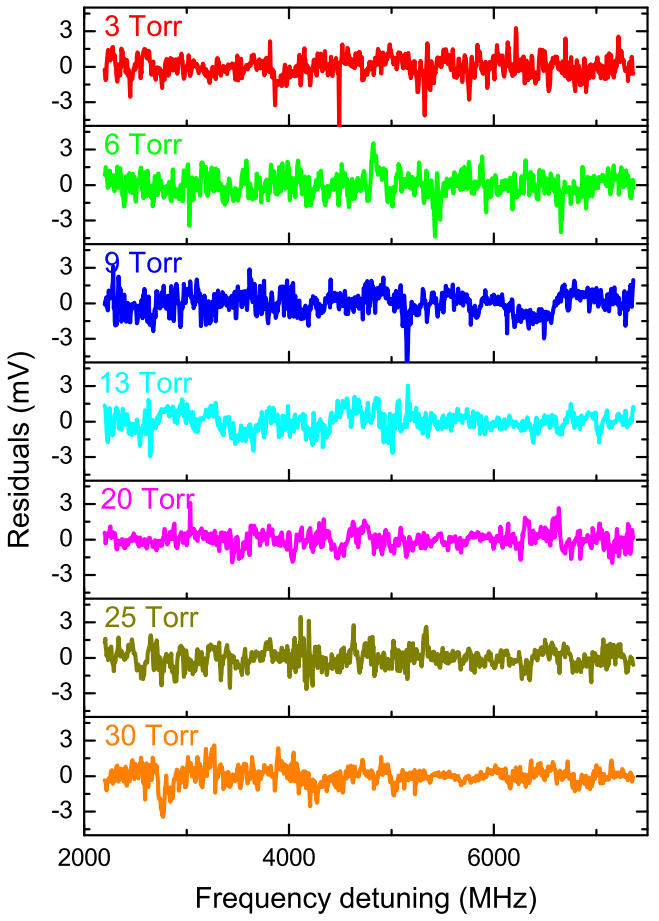


FIG. 5. Residuals resulting from the nonlinear least-squares fit of Eq. (8), for all the spectra of Fig. 4.

TABLE II. Spectroscopic parameters obtained at $T = 273.16$ K (first line) and rescaled at $T_0 = 296$ K (second line) for comparison with previous works. The quantity $\gamma_0$ was rescaled to $T_0$ using the equation $\gamma_0(T_0) = \gamma_0(T)(\frac{T}{T_0})^n$, being $n = 0.75$. Overall uncertainties, in parentheses, correspond to one standard deviation.

| S ($10^{-23}$ cm/molecule) | $\gamma_0$ ($cm^{-1}$/atm) | $\delta_0$ ($cm^{-1}$/atm) | $\gamma_2$ | $\delta_2$ | $\beta_{VC}$ ($cm^{-1}$/atm) | S ($10^{-23}$ cm/molecule)[a] | S ($10^{-23}$ cm/molecule)[b] | S ($10^{-23}$ cm/molecule)[c] |
|---|---|---|---|---|---|---|---|---|
| 1.584(3) | 0.1602(2) | −0.006746(12) | 0.1217(2) | 0.2140(6) | 0.03058(7) | | | |
| 1.555(3) | 0.1508(2) | | | | 0.02937(7) | 1.551 | 1.538 | 1.508 |

[a]Ref. [48].
[b]Ref. [19].
[c]Ref. [20].

0.15, we found that the retrieved $\beta_{VC}$ value was smaller than the calculated one, in agreement with the prediction. Instead, when considering $\eta$ as a free parameter, an overestimated value of $\beta_{VC}$ was obtained, this latter being 20% greater than the kinetic counterpart. In addition, if $\beta_{VC}$ is fixed to its upper limit and $\eta$ is treated as a free parameter, a correlation parameter of 0.2713(6) is found. This value is not physically meaningful since it would lead to a negative value for the quantity $\beta_{VC} - \eta\gamma_0$ (calculated from data of Table II).

The measured parameters are reported in Table II. For an easy comparison, data from previous studies [19,20],[1] as well as those from the HITRAN database [48], have been also listed. The transition strength value, $S$, reported in HITRAN for the $P_e(14)$ line has a relative uncertainty of 2–5%. Moreover, Jacquemart *et al.* estimated a mean accuracy for their line intensity measurements in the range between 3 and 5% for most of the investigated lines [19]. They used a multispectrum fitting procedure based on the use of the Voigt profile to calculate the absorption coefficients of the lines, fixing at some theoretically calculated values the self-broadening coefficients and setting to zero the pressure shifting effect. Our $S$ determination results in being slightly shifted towards a higher value with respect to the others, even being in good agreement with the HITRAN value [48] and with that of [19]. In contrast, the line intensity factor reported in [20] is significantly different from our determination, being the relative difference equal to ∼3%, namely, a factor of 30 bigger than their quoted uncertainty.

As far as the self-broadening coefficient is concerned, the HITRAN value is 0.141 $cm^{-1}$/atm, with a relative uncertainty in the range 2–5%. It was obtained by theoretical extrapolation from lines belonging to 15 hot bands involving the $\nu_4 = 1$ and $\nu_5 = 1$ vibrational levels [50]. Following the recommendation given in [48], we adopted a temperature-dependent exponent for $\gamma_0$ of 0.75. This latter refers to air-broadened spectra and it was shown to be noticeably dependent on $J$, the experimental determinations varying from about 0.60 to 0.85 [50]. After rescaling the measured value to the reference temperature $T_0 = 296$ K, we found a self-broadening coefficient that is ∼6% larger than the one reported in HITRAN. However, a different choice for $n$, for instance $n = 0.85$, would make our determination much closer to the HITRAN value. On the other hand, we note a good agreement with the value reported in [20], $\gamma_0 = 0.1522(2)$ $cm^{-1}$/atm (this latter being measured at 295 K).

### B. Path-length determination and line intensities retrieval

The determination of $S$ requires the knowledge of the absorption path length, $L$, and the conversion of the $C_2H_2$ pressures in molecular number densities.

The measurement of the path length inside the multiple reflection cell was carried out following the procedure already described in detail elsewhere [51]. Very briefly, we compared $L$ with a 1-m-long reference cell, which for the sake of simplicity is not shown in Fig. 1, simultaneously measuring the spectra in the multiple reflection cell and in the reference cell, in the presence of $C_2H_2$ gas samples at the same thermodynamic conditions. The spectral analysis was performed by using the symmetric version of the speed-dependent Voigt profile, in order to retrieve the integrated absorbance in the multiple reflection cell, $A^{MRC}$, and in the reference cell, $A^{REF}$. These measurements were repeated for ten different values of the gas pressure, in coincidence with the $P_e(14)$ line. A linear fit of the $A^{MRC}$ data as a function of $A^{REF}$ (shown in Fig. 6) allowed us to determine $L$, the reference cell having a length of 101.2 (1) cm. We found $L = 849$ (1) cm. The combined

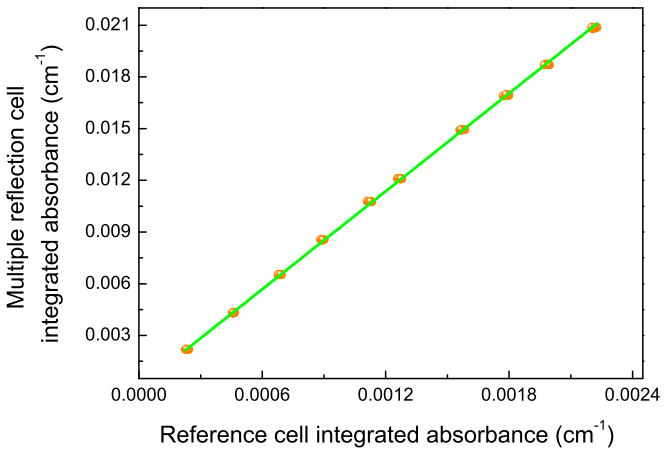


FIG. 6. Plot of the integrated absorbance in the multiple reflection cell as a function of the same quantity in the reference cell. The slope of the best-fit line is equal to the ratio between the multipass and reference cell lengths. The intercept is consistent with zero.

[1]Data reported in [19] resulted from pure $^{12}C_2H_2$ samples (with 100% of $^{12}C_2H_2$ abundance). For a proper comparison with our data and with those provided by the HITRAN database, this intensity factor has been rescaled to the atmospheric isotopic abundance $I_a = 0.977599$ [48].

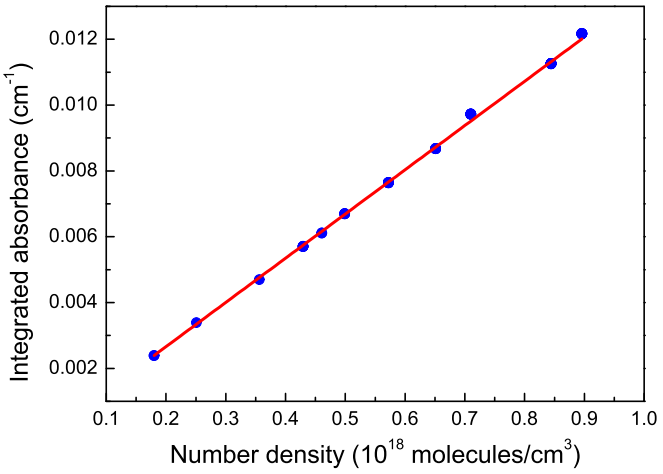


FIG. 7. Plot of the molecular number density vs the integrated absorbance. The best-fit line exhibits an excellent agreement with the experimental points. The slope of the line provides the quantity $SL$. The dispersion of the points, for each pressure, is not visible, being much smaller than the size of the points.

uncertainty resulted from a statistical contribution of 0.07% and a systematic component of 0.1%.

In Fig. 7, we report the data that allowed us to determine the transition strength. In calculating the number densities, we took into account the gas purity and the gas temperature. Furthermore, we assumed the natural isotopic abundance for $^{12}C_2H_2$ molecules (as given in the HITRAN database). For each pressure, 20 repeated measurements were performed. The experimental points (220 in total) were fitted to a straight line by using a weighted total least-squares linear regression [52], so as to consider the uncertainties on the absorbance and on the number density. In order to test the quality of the fit, we could look at the reduced $\chi_r^2$ that is equal to 0.65, for 218 degrees of freedom. If we calculate the probability $P(\chi_r^2 \geqslant 0.65)$, we find $P \sim 99.998\%$, which is much larger than any reasonable boundary (for instance 5%). The perfect agreement between the data points and the linear fit of Fig. 7 was due to two main factors: the very high experimental reproducibility in recording absorption spectra, ensured by the repeatability of the frequency scan, and the good performances of the temperature stabilization system, as already discussed in Sec. II.

Since the HITRAN value refers to the temperature $T_0$, it was necessary to rescale the retrieved $S(T)$ value to the reference temperature $T_0$, using the following equation:

$$S(T_0) = S(T)\frac{Q(T)}{Q(T_0)}\left[1-\exp\left(-\frac{hc\nu_0}{k_B T_0}\right)\right] \times \left[1-\exp\left(-\frac{hc\nu_0}{k_B T}\right)\right]^{-1} \times \exp\left[-hc\frac{E}{k_B}\left(\frac{1}{T_0}-\frac{1}{T}\right)\right], \quad (9)$$

$h$ being the Planck constant, $E$ the energy of the lower level of the transition in cm$^{-1}$, and $Q$ the total internal partition function calculated by means of the well-known polynomial approximation [53].

### C. Uncertainty budget

In this section, the complete budget of uncertainties is reported for the line intensity determination. We will distinguish among type A and type B uncertainties. The evaluation of the former is based on any valid statistical method for treating data, while type B uncertainties (including systematical deviations) are inferred from scientific judgment or other information concerning the possible values of the quantity.

Type A uncertainty is due to the statistical uncertainty of the linear fit of Fig. 7, which, in turn, takes into account the type A uncertainty on the integrated absorbance and the type B uncertainty of the molecular gas density. This latter was related to the pressure measurement, the uncertainty of which was 1% (a combination of the accuracy of our pressure gauge and the uncertainty on the sample purity of the gas sample). In contrast, the contribution to the uncertainty due to the temperature (type A and B) was completely negligible, being at the level of $1 \times 10^{-6}$. From the weighted linear fit, we quoted an overall type A uncertainty of about 0.17%.

Type B contributions are ascribed to (i) the optical path length, (ii) the detector's nonlinearity, (iii) the linearity of the frequency scale, (iv) the laser emission width, and (v) the partition function. As for the gas sample purity, we considered the fact that the $C_2H_2$ partial pressure amounted to 99.6% of the total pressure. The uncertainty on this value was included in the uncertainty on the pressure measurements; therefore, it was converted into a type A uncertainty by the weighted linear fit. The overall component associated to the optical path length resulted in 0.12% (a combination of 0.07 and 0.1% of type A and B uncertainties, respectively). Regarding the detector nonlinearity, it is useful to recall that InGaAs photodiodes show a linearity within 0.04% (at one standard deviation) over the photocurrent range from $10^{-7}$ to $10^{-4}$ A [54]. In order to quantify its influence on the integrated absorbance, we adopted the following procedure: after simulating "nonlinear" absorption spectra, we did the spectral analysis and determined the integrated absorbance, which was compared with the expected one. We found an average relative difference (over the simulated pressure range) of $3 \times 10^{-4}$. It is worth noting that the nonlinearity was considered in our simulations in the form of a frequency-dependent second-order polynomial added to the vertical scale of each simulated spectrum so that the relative deviation between original and distorted spectra was 0.04%. Similarly, the analysis of numerically simulated spectra showed that the systematical contributions due to the laser linewidth and to the linearity of the frequency scale could be neglected. In fact, thanks to the phase locking electronics, the spectral purity of the PL was at the level of a few kHz, namely, at least a factor $10^{-5}$ smaller than the width of the absorption line in the worst case. On the other hand, measuring the difference between the frequency of the rf synthesizer and that of the beat note, the nonlinearity of the frequency scan was found to be smaller than one part over $10^8$ for a 5-GHz scan.

Finally, a further source of type B uncertainty could be ascribed to the partition function. Since $Q(T)$ comes into play during the rescaling of $S$ to the reference temperature $T_0$ [see Eq. (9)], its uncertainty must be properly taken into account. Following the outcomes of [53], we found that this additional contribution amounts to 0.04%.

TABLE III. Uncertainty budget (in terms of relative contributions, corresponding to one standard deviation) for the line intensity determination.

| Contribution | Type A | Type B |
|---|---|---|
| Linear fit | 0.17% | |
| Path length | 0.07% | 0.1% |
| Linearity of frequency scale | | Negligible |
| Detector's nonlinearity | | 0.03% |
| Laser emission linewidth | | Negligible |
| Partition function | | 0.04% |
| Temperature | Negligible | 0.0012% |
| Total uncertainty | 0.22% | |

Table III summarizes the complete uncertainty budget, which leads to an overall uncertainty of 0.22%.

## V. CONCLUSIONS

The Hartmann-Tran profile was applied to the analysis of high-resolution measurements of the $C_2H_2$ absorption spectra, adopting a global fitting approach. High spectral fidelity was reached by using a dual-laser methodology. Our study evidenced the occurrence of Dicke narrowing effects and speed dependence of relaxation rates for self-colliding acetylene molecules.

The main outcome of this work is related to the level of accuracy in the retrieval of the line intensity factor. In fact, as a result of a detailed uncertainty budget, we found that the global uncertainty (at 1-$\sigma$) was equal to 0.22%, mostly limited by two factors: (i) the uncertainty in the optical path-length determination and (ii) the statistical uncertainty. We also measured the pressure broadening and shifting parameters for the $P_e(14)$ line with a precision of 0.13 and 0.18%, respectively. To the best of our knowledge, these measurements are the most accurate to date in pure $C_2H_2$ gas samples.

Our methodology can be easily extended to many other lines of different combination bands pursing the attractive idea of providing an extensive list of spectroscopic parameters. To this purpose, an optical frequency comb synthesizer could replace our reference laser, in order to have a more versatile system capable of studying lines at arbitrary frequencies.


[1] R. Whitby and E. Altwicker, Atmospheric Environment (1967) **12**, 1289 (1978).

[2] R. Zander, C. Rinsland, D. Ehhalt, J. Rudolph, and P. Demoulin, J. Atmos. Chem. **13**, 359 (1991).

[3] D. Horn, J. M. McAfee, A. M. Winer, K. C. Herr, and G. C. Pimentel, Icarus **16**, 543 (1972).

[4] P. V. Sada, G. L. Bjoraker, D. E. Jennings, G. H. McCabe, and P. N. Romani, Icarus **136**, 192 (1998).

[5] R. J. Vervack, B. R. Sandel, and D. F. Strobel, Icarus **170**, 91 (2004).

[6] M. Burgdorf, G. Orton, J. van Cleve, V. Meadows, and J. Houck, Icarus **184**, 634 (2006).

[7] J. Bishop, S. Atreya, F. Herbert, and P. Romani, Icarus **88**, 448 (1990).

[8] B. Conrath, F. M. Flasar, R. Hanel, V. Kunde, W. Maguire, J. Pearl, J. Pirraglia, R. Samuelson, P. Gierasch, A. Weir, B. Bezard, D. Gautier, D. Cruikshank, L. Horn, R. Springer, and W. Shaffer, Science **246**, 1454 (1989).

[9] K. Didriche and M. Herman, Chem. Phys. Lett. **496**, 1 (2010).

[10] N. J. Evans II, J. H. Lacy, and J. S. Carr, Astrophys. J. **383**, 674 (1991).

[11] V. Duflot, C. Wespes, L. Clarisse, D. Hurtmans, Y. Ngadi, N. Jones, C. Paton-Walsh, J. Hadji-Lazaro, C. Vigouroux, M. De Mazière, J.-M. Metzger, E. Mahieu, C. Servais, F. Hase, M. Schneider, C. Clerbaux, and P.-F. Coheur, Atmos. Chem. Phys. **15**, 10509 (2015).

[12] M. Kanakidou, B. Bonsang, J. C. Le Roulley, G. Lambert, D. Martin, and G. Sennequier, Nature (London) **333**, 51 (1988).

[13] M. de Labachelerie, K. Nakagawa, and M. Ohtsu, Opt. Lett. **19**, 840 (1994).

[14] T. J. Quinn, Metrologia **40**, 103 (2003).

[15] K. M. Yamada, A. Onae, F.-L. Hong, H. Inaba, and T. Shimizu, C. R. Phys. **10**, 907 (2009).

[16] A. Foltynowicz, T. Ban, P. Masłowski, F. Adler, and J. Ye, Phys. Rev. Lett. **107**, 233002 (2011).

[17] J. Mandon, G. Guelachvili, and N. Picque, Nat. Photon. **3**, 99 (2009).

[18] L. Gianfrani, Phil. Trans. R. Soc. London A **374**, 20150047 (2016).

[19] D. Jacquemart, N. Lacome, J.-Y. Mandin, V. Dana, H. Tran, F. Gueye, O. Lyulin, V. Perevalov, and L. Régalia-Jarlot, J. Quant. Spectrosc. Radiat. Transf. **110**, 717 (2009).

[20] O. Lyulin, J. V. Auwera, and A. Campargue, J. Quant. Spectrosc. Radiat. Transf. **160**, 85 (2015).

[21] S. Robert, B. Amyay, A. Fayt, G. D. Lonardo, L. Fusina, F. Tamassia, and M. Herman, J. Phys. Chem. A **113**, 13251 (2009).

[22] S. Arteaga, C. Bejger, J. Gerecke, J. Hardwick, Z. Martin, J. Mayo, E. McIlhattan, J.-M. Moreau, M. Pilkenton, M. Polston, B. Robertson, and E. Wolf, J. Mol. Spectrosc. **243**, 253 (2007).

[23] S. Robert, M. Herman, A. Fayt, A. Campargue, S. Kassi, A. Liu, L. Wang, G. D. Lonardo, and L. Fusina, Mol. Phys. **106**, 2581 (2008).

[24] S. Twagirayezu, M. J. Cich, T. J. Sears, C. P. McRaven, and G. E. Hall, J. Mol. Spectrosc. **316**, 64 (2015).

[25] C. McRaven, M. Cich, G. Lopez, T. J. Sears, D. Hurtmans, and A. Mantz, J. Mol. Spectrosc. **266**, 43 (2011).

[26] J.-M. Hartmann, C. Boulet, and D. Robert, *Collisional Effects on Molecular Spectra* (Elsevier, Amsterdam, 2008).

[27] J. Tennyson, P. F. Bernath, A. Campargue, A. G. Császár, L. Daumont, R. R. Gamache, J. T. Hodges, D. Lisak, O. V. Naumenko, L. S. Rothman, H. Tran, N. F. Zobov, J. Buldyreva, C. D. Boone, M. D. D. Vizia, L. Gianfrani, J.-M. Hartmann, R. McPheat, D. Weidmann, J. Murray, N. H. Ngo, and O. L. Polyansky, Pure Appl. Chem. **86**, 1931 (2014).

[28] N. Ngo, D. Lisak, H. Tran, and J.-M. Hartmann, J. Quant. Spectrosc. Radiat. Transf. **129**, 89 (2013).

[29] D. Lisak, A. Cygan, D. Bermejo, J. Domenech, J. Hodges, and H. Tran, J. Quant. Spectrosc. Radiat. Transf. **164**, 221 (2015).
[30] M. D. De Vizia, A. Castrillo, E. Fasci, P. Amodio, L. Moretti, and L. Gianfrani, Phys. Rev. A **90**, 022503 (2014).
[31] G. Larcher, X. Landsheere, M. Schwell, and H. Tran, J. Quant. Spectrosc. Radiat. Transf. **164**, 82 (2015).
[32] J. Domyslawska, S. Wójtewicz, P. Maslowski, A. Cygan, K. Bielska, R. S. Trawinski, R. Ciurylo, and D. Lisak, J. Quant. Spectrosc. Radiat. Transf. **169**, 111 (2016).
[33] A. F. Seleznev, G. V. Fedoseev, M. A. Koshelev, and M. Yu Tretyakov, J. Quant. Spectrosc. Radiat. Transf. **161**, 171 (2015).
[34] D. Forthomme, M. Cich, S. Twagirayezu, G. Hall, and T. Sears, J. Quant. Spectrosc. Radiat. Transf. **165**, 28 (2015).
[35] J. Ye, L.-S. Ma, and J. L. Hall, Opt. Lett. **21**, 1000 (1996).
[36] H. Dinesan, E. Fasci, A. Castrillo, and L. Gianfrani, Opt. Lett. **39**, 2198 (2014).
[37] H. Dinesan, E. Fasci, A. D'Addio, A. Castrillo, and L. Gianfrani, Opt. Express **23**, 1757 (2015).
[38] A. Merlone, F. Moro, A. Castrillo, and L. Gianfrani, Int. J. Thermophys. **31**, 1360 (2010).
[39] G. Casa, A. Castrillo, G. Galzerano, R. Wehr, A. Merlone, D. Di Serafino, P. Laporta, and L. Gianfrani, Phys. Rev. Lett. **100**, 200801 (2008).
[40] L. Moretti, A. Castrillo, E. Fasci, M. D. De Vizia, G. Casa, G. Galzerano, A. Merlone, P. Laporta, and L. Gianfrani, Phys. Rev. Lett. **111**, 060803 (2013).
[41] G. Casa, D. A. Parretta, A. Castrillo, R. Wehr, and L. Gianfrani, J. Chem. Phys. **127**, 084311 (2007).
[42] F. Rohart, H. Mäder, and H.-W. Nicolaisen, J. Chem. Phys. **101** 6475 (1994).
[43] F. Rohart, A. Ellendt, F. Kaghat, and H. Mäder, J. Mol. Spectrosc. **185**, 222 (1997).
[44] P. Amodio, L. Moretti, A. Castrillo, and L. Gianfrani, J. Chem. Phys. **140**, 044310 (2014).
[45] D. Benner, C. P. Rinsland, V. Devi, M. A. H. Smith, and D. Atkins, J. Quant. Spectrosc. Radiat. Transf. **53**, 705 (1995).
[46] M. R. Zaghloul and A. N. Ali, ACM Trans. Math. Softw. **38**, 15:1 (2012).
[47] J. A. C. Weideman, SIAM J. Numer. Anal. **31**, 1497 (1994).
[48] L. Rothman, I. Gordon, Y. Babikov, A. Barbe, D. C. Benner, P. Bernath, M. Birk, L. Bizzocchi, V. Boudon, L. Brown, A. Campargue, K. Chance, E. Cohen, L. Coudert, V. Devi, B. Drouin, A. Fayt, J.-M. Flaud, R. Gamache, J. Harrison, J.-M. Hartmann, C. Hill, J. Hodges, D. Jacquemart, A. Jolly, J. Lamouroux, R. J. Le Roy, G. Li, D. Long, O. Lyulin, C. Mackie, S. Massie, S. Mikhailenko, H. Müller, O. Naumenko, A. Nikitin, J. Orphal, V. Perevalov, A. Perrin, E. Polovtseva, C. Richard, M. Smith, E. Starikova, K. Sung, S. Tashkun, J. Tennyson, G. Toon, V. Tyuterev, and G. Wagner, J. Quant. Spectrosc. Radiat. Transf. **130**, 4 (2013).
[49] J. Hirschfelder, C. Curtis, and R. Bird, *Molecular Theory of Gases and Liquids* (Wiley, New York, 1964).
[50] D. Jacquemart, J.-Y. Mandin, V. Dana, L. Régalia-Jarlot, J.-J. Plateaux, D. Décatoire, and L. Rothman, J. Quant. Spectrosc. Radiat. Transf. **76**, 237 (2003).
[51] A. Castrillo, G. Gagliardi, G. Casa, and L. Gianfrani, Phys. Rev. A **67**, 062503 (2003).
[52] A. Malengo and F. Pennecchi, Metrologia **50**, 654 (2013).
[53] R. Gamache, S. Kennedy, R. Hawkins, and L. Rothman, J. Mol. Struct. **517-518**, 407 (2000).
[54] H. W. Yoon, J. J. Butler, T. C. Larason, and G. P. Eppeldauer, Metrologia **40**, S154 (2003).